Fluorinated Mn(III)/(II)-Porphyrin with Redox-Responsive 1 H and 19 F Relaxation Properties

Sara Pinto, Ana Ferreira, Daniela Teixeira, Sandra Nunes, Ana Batista de Carvalho, Joseany Almeida, Zoltan Garda, Agnés Pallier, Alberto Pais, Christopher Brett, et al.

RESEARCH ARTICLE

Fluorinated Mn(III)/(II)-Porphyrin with Redox-Responsive ^{1}H and ^{19}F Relaxation Properties

Sara M.A. Pinto* [a,b], Ana R.R. Ferreira [a,b], Daniela S.S. Teixeira[a,b], Sandra C.C. Nunes [a,b], Ana L.M. Batista de Carvalho[c,d], Joseany M. S. Almeida[a,e], Zoltan Garda[f], Agnés Pallier[f], Alberto A.C.C. Pais [a,b], Christopher M.A. Brett[a,e], Éva Tóth*[f], Maria P.M. Marques[c,d], Mariette M. Pereira[a,b] and Carlos F.G.C. Geraldes*[b,d,g]

[a] Dr. Sara M.A. Pinto, Ana R.R. Ferreira, Daniela S.S. Teixeira, Dr. Sandra C.C.Nunes, Dr. Alberto A.C.C. Pais, Dr. Joseany M.S. Almeida, Dr. Christopher M.A. Brett, Dr. Mariette M. Pereira
Department of Chemistry, University of Coimbra, Rua Larga Largo D. Dinis, 3004-535 Coimbra, Portugal
E-mail: smpinto@qui.uc.pt

[b] Dr. Sara M.A. Pinto, Ana R.R. Ferreira, Daniela S.S. Teixeira, Dr. Sandra C.C. Nunes, Dr. Alberto A.C.C. Pais, Dr. Mariette M. Pereira, Dr. Carlos F.G.C. Geraldes
Coimbra Chemistry Center, University of Coimbra, Rua Larga Largo D. Dinis, 3004-535 Coimbra, Portugal
E-mail: geraldes@ci.uc.pt

[c] Dr. Ana L.M. Batista de Carvalho, Dr. Maria P.M. Marques, Dr. Carlos F.G.C. Geraldes
Molecular Physical Chemistry R&D Unit, Department of Chemistry, University of Coimbra, Rua Larga, 3004-535 Coimbra, Portugal

[d] Dr. Ana L.M. Batista de Carvalho, Dr. Maria P.M. Marques, Dr. Carlos F.G.C. Geraldes
Department of Life Sciences, Faculty of Science and Technology, Calçada Martim de Freitas, 3000-393 Coimbra, Portugal.

[e] Dr. Joseany M.S. Almeida, Dr. Christopher M.A. Brett, CEMMPRE, University of Coimbra, Pinhal de Marrocos, 3030-788 Coimbra, Portugal

[f] Dr. Zoltan Garda, Dr. Agnés Pallier, Dr. Éva Tóth
Centre de Biophysique Moléculaire, CNRS, UPR 4301, Université d'Orléans, Rue Charles Sadron, 45071 Orléans Cedex 2, France.
E-mail: eva.jakabtoth@cnrs.fr

[g Dr. Carlos F.G.C. Geraldes
CIBIT/ICNAS, University of Coimbra, Azinhaga de Santa Comba, 3000-548, Coimbra, Portugal

Abstract: A new fluorinated manganese porphyrin, (Mn-TPP-*p*-CF_3) is reported capable of providing, based on the Mn(III)/Mn(II) equilibrium, dual ^{1}H relaxivity and ^{19}F NMR response to redox changes. The physical-chemical characterization of both redox states in DMSO-d_6 evidenced that the ^{1}H relaxometric and ^{19}F NMR properties are appropriate for differential redox MRI detection. The Mn(III)-F distance (d_{Mn-F} = 9.7 - 10 Å), as assessed by DFT calculations, is well tailored to allow for adequate paramagnetic effect of Mn(III) on ^{19}F T_1 and T_2 relaxation times. Mn-TPP-*p*-CF_3 has a reversible Mn(II)/Mn(III) redox potential 0.574 V vs. NHE in deoxygenated aqueous HEPES/ THF solution. The reduction of Mn(III)-TPP-*p*-CF_3 in the presence of ascorbic acid is slowly but fully reversed in the presence of air oxygen, as monitored by UV-Vis spectrometry and ^{19}F NMR. The broad ^{1}H and ^{19}F NMR signals of Mn(III)-TPP-*p*-CF_3 disappear in the presence of 1 equivalent ascorbate replaced by a shifted and broadened ^{19}F NMR signal from Mn(II)-TPP-*p*-CF_3. Phantom ^{19}F MR images in DMSO show a MRI signal intensity decrease upon reduction of Mn(III)-TPP-*p*-CF_3, retrieved upon complete reoxidation in air within ~24 hours. ^{1}H NMRD curves of the Mn(III)/(II)-TPP-*p*-CF_3 chelates in mixed DMSO/water solvent have the typical shape of Mn(II)/Mn(III) porphyrins.

Introduction In healthy tissues, both extracellular and intracellular redox environments are tightly regulated.[1,2] Their alterations due to the reduction of O_2 levels have been associated with several pathologies, including chronic inflammation[3], tissue ischemia[4], inflammation and neoplastic growth.[5] Therefore, the detection of hypoxic cells is crucial for early diagnosis allowing early disease treatment.[6] To date, potential redox probes have been described for several imaging methodologies.[7,8,9] ^{64}Cu(II)-ATSM (ATSM = diacetyl-bis(*N*^{4}-methylthiosemicarbazone) and ^{18}F-MISO (MISO = misonidazol) are well-known positron emission tomography (PET) radiotracers that have demonstrated high capability to detect hypoxic cells.[10,11,12] Metal-based redox probes have also been proposed for magnetic resonance imaging (MRI).[9,13,14,15] For instance, Loving et al[16,17] reported potential MRI redox probes based on hydroxybenzylenediamine acetic acid coordinated with manganese. These structures showed rapid and reversible interconversion between the two manganese (II/III) oxidation states, in the presence of hydrogen peroxide (oxidation) and *L*-cysteine or glutathione (reduction), with a 9-fold relaxivity increase from Mn(III) to Mn(II) analogues (at 1.41 T, 37 °C). In 2019, Pinto et al[18] proposed a biocompatible redox MRI probe based on a tetra-pegylated Mn porphyrin. This complex was capable to reversibly switch between Mn(III)/Mn(II) oxidation states in the presence of ascorbate or *β*-mercaptoethanol, with subsequent oxidation with O_2. The reduction of the Mn(III) to the Mn(II) complex was accompanied by an significant r_1 relaxivity increase, amounting to ~100 % at medium frequencies (20-40 MHz), which demonstrates its potential as a “turn on” redox MRI probe for ascorbate detection.

Despite the advantageous features of ^{1}H MRI, such as high spatial resolution and deep penetration of soft tissues, the high concentration of water in the organism may cause background interference, leading to low contrast. In the last years, ^{19}F MRI has emerged as a promising complementary technique to ^{1}H MRI,[19,20,21] minimizing the problem associated with the background signal of bulk water, as fluorinated compounds are almost absent in the human body, except for teeth and bones, where they are present as solid salts.[22,23] Such contrast agents provide ^{19}F MR images with no background which improves the signal-to-noise ratio (SNR). The ^{19}F nucleus has other advantages, such as a high gyromagnetic ratio (40.05 MHz/T), 100 % isotopic abundance, non-quadrupolar nature (I = 1/2), a wide chemical shift range of ≅ 350 ppm) and high sensitivity (83 % of ^{1}H). Fluorinated compounds have relatively long relaxation times, leading to long image acquisition.[23] Hence, introduction of a paramagnetic ion, either a transition metal ion like Co(II) [24] or a lanthanide metal ion,[25,26,27,28,29,30] close to the ^{19}F nuclei, will shorten both T_1 and T_2 relaxation times through the paramagnetic relaxation enhancement (PRE) effect.[26] This will have contradictory effects on ^{19}F MRI: while T_1 shortening decreases acquisition times, reducing T_2 causes signal broadening which decreases signal intensity, sensitivity and final image resolution. Therefore, optimal probes should have a $T_2/T_1 \cong 1$. Besides the PRE effect, metal ions with anisotropic unpaired electrons can induce changes in the ^{19}F chemical shift through pseudo-contact shift (PCS) effects. [31]

Although the development of potential fluorinated probes has undergone a large growth in recent years, only a few redox ^{19}F MRI probes have been reported until now. [31] Que's group [24,32,33] reported a series of fluorinated Cu(II)ATSM derivatives that, through the reduction of paramagnetic Cu(II) (S=1/2) to diamagnetic Cu(I), acted as "turn on" ^{19}F NMR probes through the disappearance of the PRE and PCS effects. The same group [34] reported a fluorinated Co(II)NOTA (NOTA = 1,4,7-triazacyclononane-1,4,7-triacetic acid) complex, in which the conversion of paramagnetic high spin Co(II) (S=3/2) to diamagnetic low spin Co(III) (S=0) was observed upon oxidation with H_2O_2. This change in the oxidation state of cobalt resulted in a ^{19}F NMR chemical shift change through a PCS effect and enhancement in the ^{19}F NMR signal through a PRE effect. A Fe(III)/Fe(II) dendrimer [35] and a Eu(III)/Eu(II) macrocyclic complex [36] were also described as ^{19}F NMR redox probes. Recently, Chen et al[37] reported a water soluble, redox responsive Mn(III) (S=2)/Mn(II) (*S*=5/2) complex that smoothly responded to biological redox active species, like glutathione, resulting in a change in signal intensity in ^{19}F NMR and ^{1}H/^{19}F MRI. Nevertheless, despite the favorable features of the complexes mentioned above, they may present some unfavorable issues, such as lack of biocompatibility, thermodynamic stability and kinetic inertness and non-ideal half-cell potential. [9,16]

Porphyrins are tetrapyrrolic macrocycles, well known for their physico-chemical and biological features that make them appealing in a multitude of applications, such as catalysis [38,39,40], materials science [42,42,43] and biomedicine [44,45,46] including MRI.[18,47,48] The capability of the porphyrin ligand to coordinate several metal ions, especially those of manganese, has been extensively studied.[49,50] The Mn(III) ion fits perfectly in the porphyrin cavity, where its octahedral coordination is ensured through strong bonds with the equatorial N4 atoms of the porphyrin and relatively weakly with the axial ligands.[51,52] Also, manganese is a biogenic element, present in both paramagnetic +2 and +3 oxidation states allowing for MRI contrast agent use. Mn^{2+} possesses a $3d^5$ configuration (high spin S = 5/2), long (0.1–1 ns) longitudinal electronic relaxation times ($T_{1,2e}$) and labile inner-sphere water, being a very efficient paramagnetic relaxation agent, while Mn^{3+}, with a $3d^4$ configuration (high spin S = 2), has fast water exchange,[53] shorter $T_{1,2e}$ values (≤10 ps), typically making it a less efficient relaxation agent.[54]

Previously, we have demonstrated the capability of a Mn(III)/Mn(II) porphyrin to provide an important ^{1}H relaxivity response to redox changes.[18] With the objective of extending the potential of such compounds to dual ^{1}H and ^{19}F detection, we describe here the synthesis and the detailed physical-chemical characterization of a new a fluorinated manganese porphyrin, (Mn-TPP-*p*-CF_3). Although Mn-TPP-*p*-CF_3 is insoluble in aqueous media, it is an interesting model compound to better understand the structural features required in particular for ^{19}F redox reporters based on manganese porphyrins. We report here the ^{1}H and ^{19}F NMR properties for both redox states. Mn(III)-F distances are of primary importance for the paramagnetic relaxation enhancement effect, therefore they were assessed by DFT calculations and were related to experimental ^{19}F relaxation rate measurements. For comparison, the same was also performed for Mn(III)-TFPP porphyrin (see structure in SI (Figure S1), which has a fluorine atom in the *ortho* position of the phenyl group. The redox properties of the Mn-TPP-*p*-CF_3 complex were studied by cyclic voltammetry, and UV-Vis spectrophotometry was used to follow the kinetics of Mn(III) reduction in the presence of ascorbate and Mn(II) re-oxidation in the presence of atmospheric oxygen. For both redox forms, ^{1}H relaxivities were measured in water/DMSO mixture and ^{19}F MRI images were acquired. Evaluation of the antiproliferative effect of Mn(III)-TPP-*p*-CF_3 towards the Caco-2 epithelium cell line, which measures its capacity of causing cell cycle arrest or delay and DNA degradation, is also reported. These measurements are aimed to assess the compound´s potential as an anticancer drug, aiming at a multimodal agent (diagnostic + therapeutics). Overall, these data can help the future design of more biocompatible and more efficient Mn porphyrins as dual ^{1}H and ^{19}F MRI probes for redox detection.

Results and Discussion

Synthesis

The strategy adopted for the synthesis of the fluorinated Mn(III) complex, Mn(III)-TPP-*p*-CF_3, is depicted in Scheme 1. The synthesis of 5,10,15,20-tetrakis(4-trifluoromethylphenyl)porphyrin, TPP-*p*-CF_3, was performed with adaptation of the NaY/nitrobenzene methodology[55,56]. After precipitation with methanol and filtration under vacuum, porphyrin TPP-*p*-CF_3 was obtained in 20% yield. The preparation of porphyrin Mn(III)-TPP-*p*-CF_3 proceeded by reacting free base porphyrin TPP-*p*-CF_3 with excess of manganese diacetate tetrahydrate in sodium acetate/acetic acid buffer solution, at 80°C, for two hours. After performing the workup of the crude, the Mn(III)-TPP-*p*-CF_3 porphyrin was obtained in 85% yield. The purity of Mn(III)-TPP-*p*-CF_3 was evaluated by HPLC, giving 98% purity (Figure S2).

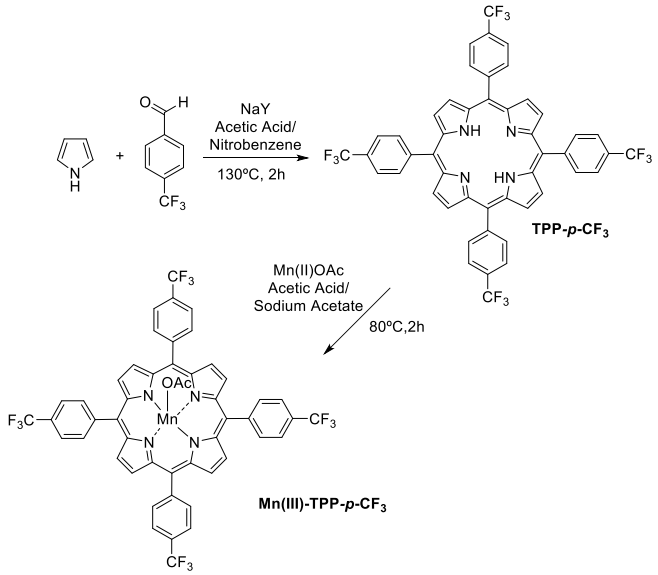

Scheme 1. Synthetic route for the preparation of porphyrin Mn(III)-TPP-*p*-CF_3

^{1}H and ^{19}F NMR and relaxivity and DFT calculations

^{1}H and ^{19}F NMR spectra of TPP-*p*-CF_3 and Mn(III)-TPP-*p*-CF_3 were acquired in DMSO-d_6. The ^{1}H NMR of TPP-*p*-CF_3 (Figure S6a) shows a singlet at 8.82 ppm (*β*-pyrrolic protons) and two doublets at 8.34 ppm and 8.05 ppm, assigned, respectively, to the *ortho* and *meta* protons of the porphyrin *meso* aryl group. As expected, the introduction of the paramagnetic Mn(III) ion,[57,58,59] causes a strong broadening of the aryl proton signals which collapse into a single broad resonance at δ=7.85 ppm. (Figure S6b).

Figure 1 shows the ^{19}F NMR spectra of TPP-*p*-CF_3, Mn(III)-TPP-*p*-CF_3 and Mn(II)-TPP-*p*-CF_3 at -61.04 ppm, -61.42 ppm and -59.61 ppm, respectively. The introduction of Mn(III) into the porphyrin broadens the ^{19}F NMR signal which remains nevertheless well detectable, providing the first indication that this porphyrin complex might be suitable as a ^{19}F MRI probe. Reduction of Mn(III)-TPP-*p*-CF_3 to Mn(II)-TPP-*p*-CF_3 results in further line-broadening, in accordance with the stronger relaxation effect of Mn(II). PCS values of -0.38 and +1.43 ppm are observed with respect to the free porphyrin ligand for the Mn(III)-TPP-*p*-CF_3 and Mn(II)-TPP-*p*-CF_3 complexes, respectively.

The distance between the fluorine atoms and the paramagnetic ion (d_{Mn-F}) is crucial in determining both the PCS ((d_{Mn-F})$^{-3}$ dependence) and the PRE effect ((d_{Mn-F})$^{-6}$ dependence).[21,23,26] If the two atoms are too close, the paramagnetic effect on the ^{19}F T_2 relaxation time will be severe, causing excessive broadening, while if they are too distant, the T_1 and T_2 relaxation times will not be significantly affected. Since it was not possible to obtain single crystal DFT was used for Mn-F distance calculations

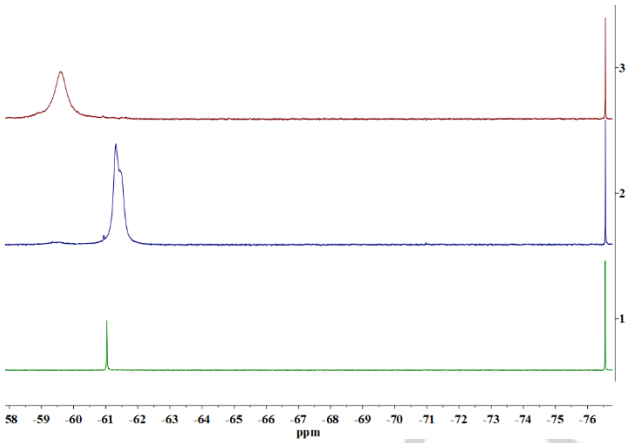

Figure 1. ^{19}F NMR of 1) TPP-*p*-CF_3; 2) Mn(III)-TPP-*p*-CF_3 and 3) Mn(II)-TPP-*p*-CF_3 in DMSO. The peak at -76.55 ppm corresponds to NaTFA as reference.

In order to relate ^{19}F relaxation properties to the molecular structure, the Mn-F distance has been calculated for Mn(III)-TPP-*p*-CF_3, with CF_3 in *para* position of the aryl group (*ph*), as well as for another porphyrin complex, Mn(III)-TFPP (see structure in SI), in which d_{Mn-F} is considerably shorter. Both structures were fully optimized at the B3lyp/6-31G(d,p) level.

For each molecule, different starting structures were considered varying both the dihedral that defines the positioning of the *ph*-CF_3 and *ph*-F groups relatively to the porphyrin plane and the positioning of the F atoms relatively to the OAc group in the Mn(III)-TFPP complex. For this molecule, different conformers were optimized considering all the arrangements of the F atoms relatively to the OAc group, namely those in which all the F atoms are on the same side (relatively to the porphyrin plane) of the acetate group, those in which the fluorine atoms are in the opposite side of the OAc group and those in which only one, two or three F atoms are on the same side of the OAc group. It was found that the energy differences obtained are below 7.5 kJ/mol among the different conformers, both for Mn(III)-TPP-*p*-CF_3 and Mn(III)-TFPP. The most stable structures obtained for each molecule are depicted in Figure 2. Electronic energy values and optimized structures calculated for all conformers are given in the Supporting Information (Table S1, Figures S3 and S4). In the optimized structures of both complexes, the substituent groups of the porphyrin adopt an arrangement almost perpendicular to the porphyrin plane in all conformers. The dihedrals that define the positioning of *ph*-CF_3 groups relatively to the porphyrin plane have values between 70 and 112°, while in the case of *ph*-F groups the corresponding dihedrals vary between 69 and 109°. It should be mentioned that for Mn(III)-TFPP the most stable structure presents two fluorine atoms facing upwards and two facing downwards relatively to the porphyrin plane. In both complexes a weak CH…O hydrogen bond, established between a CH group of the phenyl groups and the oxygen atom of the carbonyl group, seems to contribute to the stabilization of the structures, while in some conformers of Mn(III)-TFPP a CH…F hydrogen bond, established between the CH_3 group of the OAC moiety and the F atoms, may also contribute to the stabilization of the complex.

As expected, the Mn(III)-^{19}F distances (d_{Mn-F}) were found to be considerably different for the two complexes: they vary between 9.7 and 10 Å for Mn(III)-TPP-*p*-CF_3 and between 5.1 and 5.8 Å for

Mn(III)-TFPP. The almost double Mn(III)-^{19}F distances in Mn(III)-TPP-*p*-CF_3 have a very strong effect on the ^{19}F T_1 and T_2 relaxation times, as determined experimentally for the two Mn(III) chelates at 9.4 T, in comparison to the non-metalated porphyrin **1** (Table 1).

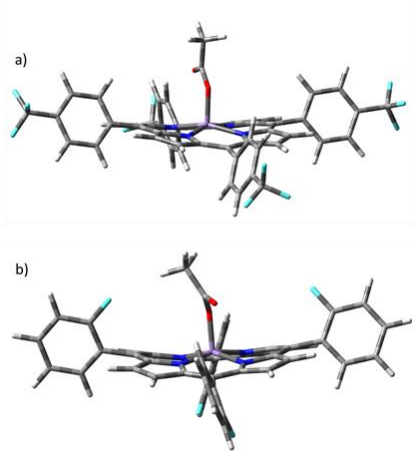

Figure 2. Most stable structures obtained through optimization at the B3LYP/6-31G(d,p) level, of a) Mn(III)-TPP-*p*-CF_3 and b) Mn(III)-TFPP. Color code: gray, carbon; red, oxygen; blue, nitrogen; white, hydrogen; light blue, fluorine; and purple, manganese.

Table 1. Relaxation times, relaxation rates and T_2/T_1 ratios for 1, 2, TFPP and Mn(III)-TFPP. B = 9.4 T, in DMSO, 298 K (n=3)

Porphyrin	T_1 (ms)	R_1 (s^{-1})	T_2 (ms)	R_2 (s^{-1})	T_2/T_1
TPP-*p*-CF_3	968±5	1.0±0.05	325±2	3.1±0.02	0.34±0.002
Mn(III)-TPP-*p*-CF_3	11.5±0.2	87.0±1.5	7.7±0.3	130±5	0.67±0.03
Mn(II)-TPP-*p*-CF_3	6.5±0.3	154±7	1.9±0.1	526±28	0.29±0.02
TFPP	608±5	1.7±0.01	280±25	3.6±0.3	0.46±0.04
	791±5[a]	1.3±0.01	520±50[a]	1.9±0.2	0.66±0.07
Mn(III)-TFPP	0.39±0.02	2560±130	0.31±0.03	3230±300	0.80±0.07

[a] measured in $CHCl_3$

First, the data in Table 1 demonstrate that the introduction of Mn(III) or Mn(II) into TPP-*p*-CF_3 results in a considerable decrease of the ^{19}F relaxation times, due to the paramagnetic relaxation induced by the metals. This paramagnetic contribution, which is proportional to $(d_{Mn\text{-}F})^{-6}$, is particularly significant for the longitudinal relaxation ($R_{iM}=R_{ip}-R_{id}$, i=1,2, where R_{ip} and R_{id} are the observed rates for the paramagnetic complex and the diamagnetic ligand, respectively; R_{1M}=87.0 s^{-1} and R_{1M}=153.8 s^{-1} for Mn(III) and Mn(II), respectively. The substantial increase of R_1 without an excessive effect on R_2 is indicative of the potential of structures like Mn(III)-TPP-*p*-CF_3 for ^{19}F MRI, with appropriate Mn-F distance. To allow the acquisition of sufficient signal intensity in reasonable time, T_2/T_1 values should be the closest possible to 1.[21,23] In contrast, for Mn(III)-TFPP, the effect on R_1 and R_2 relaxation rates is more severe. Correspondingly, as shown in Figure S6 – SI, the addition of Mn(III) to TFPP leads to a strong broadening of the ^{19}F signals, more important than what was observed for porphyrin 2 (Figure 1 b). Altogether, these data indicate that the $d_{Mn\text{-}F}$ distance in Mn(III)-TPP-*p*-CF_3 is more appropriate to sufficiently decrease the ^{19}F T_1 value of the CF_3 substituents, allowing the reduction of the acquisition time, without deleterious T_2 shortening.

To describe the relaxation of ^{19}F nuclei in non-viscous solutions of paramagnetic complexes, the most widely used framework is the Bloch–Redfield–Wangsness (BRW) theory. For Gd-complexes, Botta, Platas-Iglesias et al have recently considered that the dipolar contribution dominates ^{19}F relaxation:

$$R_1 \cong \frac{1}{T_1^{DD}} = \frac{2}{15}\left(\frac{\mu_0}{4\pi}\right)^2 \frac{\hbar^2\gamma_S^2\gamma_I^2}{r_{MnF}^6} S(S+1)\left[\frac{3\tau_{d1}}{1+\omega_I^2\tau_{d1}^2} + \frac{7\tau_{d2}}{1+\omega_S^2\tau_{d2}^2}\right]$$

$$R_2 \cong \frac{1}{T_2^{DD}} = \frac{1}{15}\left(\frac{\mu_0}{4\pi}\right)^2 \frac{\hbar^2\gamma_S^2\gamma_I^2}{r_{MnF}^6} S(S+1)\left[\frac{3\tau_{d1}}{1+\omega_I^2\tau_{d1}^2} + \frac{13\tau_{d2}}{1+\omega_S^2\tau_{d2}^2} + 4\tau_{d1}\right]$$

Where S is the electron spin (S=5/2 for Mn^{2+} and 4/2 for Mn^{3+}), γ_I is the nuclear gyromagnetic ratio, g is the electron g factor, μ_B is the Bohr magneton, r_{MnF} is the nuclear-spin–electron-spin distance, and ω_I and ω_S are the nuclear and electron Larmor frequencies. The correlation times τ_{di} depend on the rotational correlation time, τ_R, and the electron spin relaxation times, T_{ie}.

$$\frac{1}{\tau_{di}} = \frac{1}{\tau_R} + \frac{1}{T_{ie}}$$

If we assume that at high magnetic fields the longitudinal electron spin relaxation rate can be neglected as compared to the tumbling rate of the molecule, one can estimate the rotational correlation time, τ_R, of the complexes, by using the Mn-F distances calculated from DFT. This very rough estimation gives 760±50 ps for Mn(II/III)-TPP-*p*-CF_3 and 145±5 ps for Mn(III)-TFPP. The value for Mn(II/III)-TPP-*p*-CF_3 is rather long for a small molecular complex, and might be indicative of aggregation also in pure DMSO, as it was observed in DMSO/water mixture in the NMRD measurements and by DLS data (see below).

Cyclic Voltammetry

The electrochemical behavior of the porphyrin Mn(III)-TPP-*p*-CF_3 was investigated in a deoxygenated mixture of 0.1 M HEPES buffer solution, pH 7.4 and THF, by cyclic voltammetry. Prior to CV measurements, the oxygen was removed by N_2 bubbling to avoid the influence of dissolved oxygen reduction in the electrolyte medium. The cyclic voltammograms obtained in the absence and presence of the Mn(III) porphyrin are presented in Figure 3. The electrolyte without porphyrin (blank) shows no response signal in the potential region investigated.

No evidence of Mn(III)-TPP-*p*-CF_3 adsorption was observed in consecutive cycles. In the potential range investigated, which is limited by solvent reduction and oxidation, three redox couples I_a/I_c, II_a/II_c and III_a/III_c appeared. The I_a/I_c couple, E^m_{pl} = -0.007 V vs. NHE and ΔE_{pl} = 0.124 V, can be assigned to a one-electron oxidation/reduction process of the porphyrin ring, as suggested in the literature. [60]

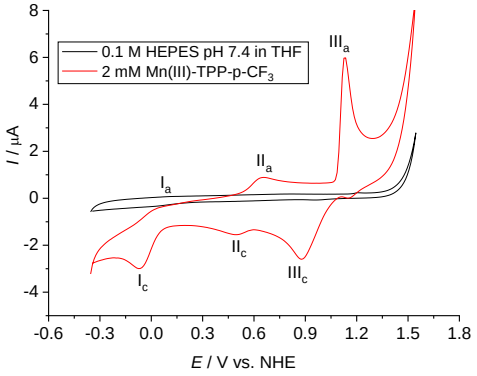

Figure 3. CVs at the GCE in 1.5 mL of 0.1 M HEPES buffer, pH 7.4 + 500 µL THF (black), for 2.0 mM Mn(III)-TPP-*p*-CF_3 (red).

The II_a/II_c pair with E^m_{pII} = 0.574 V vs. NHE and ΔE_{pII} = 0.159 V was assigned to the Mn^{II}/Mn^{III} redox process, while III_a/III_c with with E^m_{pIII} = 1.005 V vs. NHE and ΔE_{pIII} = 0.250 V was associated with the Mn^{III}/Mn^{IV} couple. As observed by Ruhlmann et al. [61], when the GCE was used in aqueous medium, at pH 12, in the evaluation of Mn(III) porphyrin, the *meso* heterodimers 3-2 and 4-2 showed reversible one-electron redox waves for the pairs Mn^{II}/Mn^{III} and Mn^{III}/Mn^{IV}. The redox potentials were close to those of meso-pyridiniumporphyrin.[62]In our studies, carried out at pH 7.4, similar redox pairs were also observed with higher current intensities for the Mn^{III}/Mn^{IV} redox pair. Comparison of the E^m_{pII} = 0.574 V vs. NHE for the Mn^{II}/Mn^{III} redox process in Mn(III)-TPP-p-CF_3 with those reported for other fluorinated porphyrins, namely Mn(III)-TPFPP(PEG)$_4$ (+0.193 V vs. NHE in PBS) with two ortho and two meta phenyl F atoms[18], Mn(III)-TPFPP (+0.050 V vs. NHE in acetonitrile) with perfluorinated phenyl groups[63] and Mn(III)-TDFPP (+0.090 V vs. NHE in acetonitrile) with two ortho phenyl F atoms[64], illustrate the effect of the number and position of the F substituents relative to the Mn(III) ion on the reduction of their redox potential. Pinto et al.[18], shows in Fig. S7d, of SI, the analysis of MnIII-TPFPP(PEG)$_4$ in dichloroethane (DCE) and in Table S1 the E1/2 several other MnPs, analyzed in different media. For the study done in DCE the redox process of the MnIII/MnII centre in the MnIII-3 porphyrin was observed at Emp = +0.335 V vs. NHE, with a peak separation ΔEp = 0.350 V. Other work also reports more positive E1/2 values when it comes to MnPs (see Table 1 of paper Batinic-Haberle et al.)[65]. This is consistent with the biologically compatible E1/2 range of the MnIIIP/MnIIP redox couple (which can vary from approximately +100 to +400 mV vs. NHE), in addition to the contribution of the electrolyte environment, which can cause shifts in this region.

The cyclic voltammetric behaviour of the porphyrin Mn(III)-TPP-*p*-CF_3 was investigated over a range of scan rates from 10 to 100 mV s^{-1}, Figure S5a. The results showed a linear dependence of the anodic and cathodic peak currents of the redox couple Mn^{II}/Mn^{III} on the square root of the scan rate (v) (Figure S5b), indicating a diffusion-controlled electron transfer process. A similar response was observed in published work with other porphyrins. [18]

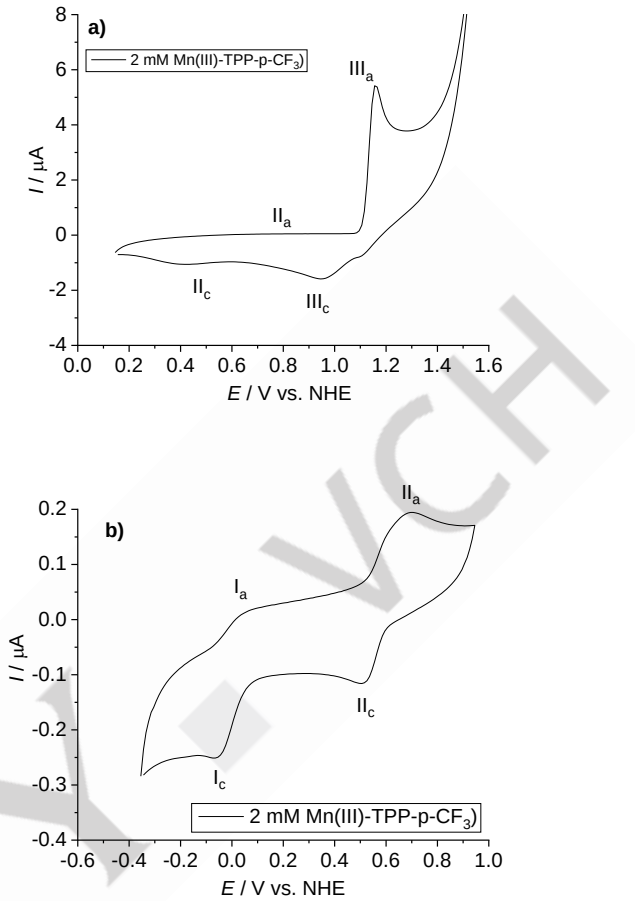

Figure 4. (a) CV for 2.0 mM of Mn(III)-TPP-*p*-CF_3 (black) in the potential range 0.2 V to 1.5 V vs. NHE, scan rate 100 mV s^{-1}. (b) CV for 2.0 mM Mn(III)-TPP-*p*-CF_3 (black) in the potential range -0.3 V to 0.9 V vs. NHE, scan rate 100 mV s^{-1} showing the Mn^{II}/Mn^{III} and redox process of the porphyrin ring.

Figure 4 shows the voltammetric response of the Mn(III)-TPP-*p*-CF_3 porphyrin couples using two different potential ranges (0.2 V to 1.5 V vs. NHE (Figure 4a) and -0.3 V to 0.9 V vs. NHE (Figure 4b)) and confirms that the peaks II_a/II_c and III_a/III_c refer to Mn^{II}/Mn^{III} and Mn^{III}/Mn^{IV}, respectively. Figure S6a and S6b. depict the corresponding variation of current with scan rate in the range 10 – 100 mV s^{-1}. The process is diffusional for both manganese redox couples, since plots of peak current vs. the square root of the scan rate (v) are linear (Figure S6c and S6d).

Figure 5 displays the CV responses of Mn(III)-TPP-*p*-CF_3 (black) and Mn(III)-acetate (red), which enabled confirmation of the peak assignment of the III_a/III_c couple to Mn(III). The potential values exhibited were $E^m_{pIII'}$ = 0.990 V vs. NHE and $\Delta E_{pIII'}$ = 0.254 V for Mn(III)-acetate, similar to those for the same couple in the porphyrin Mn(III)-TPP-*p*-CF_3.

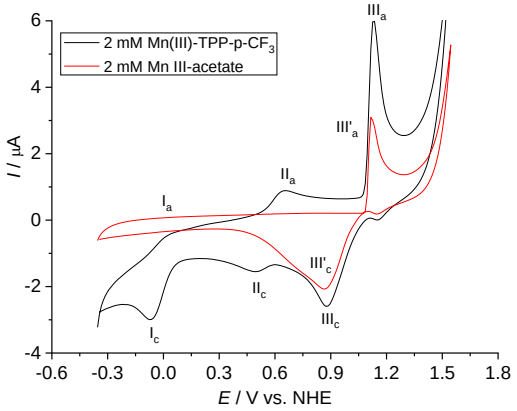

Figure 5. Cyclic voltammetry at GCE in 1.5 mL of 0.1 M HEPES buffer, pH 7.4 + 500 µL THF for (black) 2.0 mM of Mn(III)-TPP-*p*-CF_3 and (red) Mn(III)-TPP-*p*-CF3 + Mn(III)-acetate, scan rate 100 mV s^{-1}.

No signals were observed for the couple II_a/II_c in the conditions evaluated for Mn(III)-acetate. Nevertheless, concerning porphyrin Mn(III)-TPP-*p*-CF_3, the redox couple II_a/II_c presented well-defined, reversible signals for Mn^{II}/Mn^{III}, indicating that, in the porphyrin complex, manganese increases the reversibility of the Mn^{II}/Mn^{III} process. In fact, the introduction of a metal ion in the porphyrin led to a negative potential shift of these peaks, due to its effect on the electronic structure of the macrocyclic ring, as observed by Pinto et al. [18].

Biologically compatible E1/2 of the MnIIIP/MnIIP redox couples range from approximately +100 to +400 mV vs. NHE, which makes such compounds electron-deficient and allows them to bind and react with a variety of biologically relevant species. [6]. The E1/2 value of MnPs allows them to accept and donate electrons, acting as both antioxidants and pro-oxidants. Such actions are most obvious in the catalysis of dismutation of O2•-, which occurs in two stages. It is very likely that many other reactions are possible *in vivo*.[66,67]

Mn(III)/Mn(II) redox conversion

Ascorbate was used as biological reductant to evaluate the reduction of Mn(III)-TPP-*p*-CF_3 porphyrin to Mn(II)-TPP-*p*-CF_3. This reduction was followed by observing the change in the UV-Vis spectra of Mn(III)-TPP-*p*-CF_3 upon addition of increasing amounts of ascorbic acid in PBS (ascorbic acid is present as the ascorbate anion; Figures 6a and 6b). The studies were performed using THF and DMSO as solvents, for which all the solutions, including ascorbic acid in PBS, were previously desaerated and all the UV-Vis spectra were recorded under oxygen free conditions.

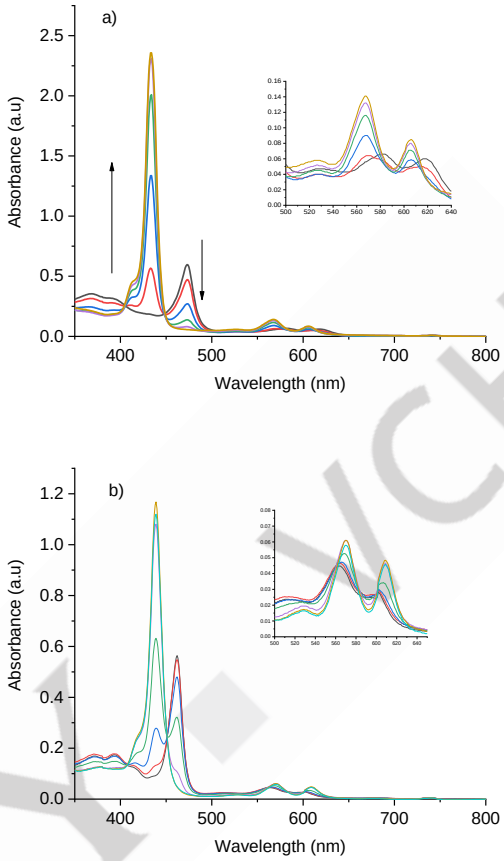

Figure 6. UV-Vis titration of 0.00426 mM of Mn(III)-TPP-*p*-CF_3 with ascorbate , recorded at 25ºC: a) in THF; number of equivalents: 0 (black line), 1 (2µL) (red line), 2 (4µL) (blue line), 4 (8µL) (green line), 6 (12µL) (purple line); 10 (20µL) (yellow); b) in DMSO: number of equivalents: 0 (black line), 1 (2µL) (red line), 2 (4µL) (blue line), 3 (6µL) (green line), 4 (8µL) (purple line), 5 (10µL) (yellow), 6 (12µL) (light blue).

The addition of ascorbic acid in PBS to the Mn(III)-TPP-*p*-CF_3 solution clearly changed the oxidation state of the porphyrin complex from Mn(III) to Mn(II), in both solvents. The addition of 1 equivalent (Figure 6a, THF) and 2 equivalents (Figure 6b, DMSO) induced a decrease in the absorption at 473 nm and 462 nm, respectively, which is the typical wavelength range for the charge transfer Soret band of Mn(III) porphyrins, with the concomitant appearance of a new band at 432 nm and 438 nm, the typical absorption wavelength of the Soret band for Mn(II) porphyrins.[50] Total reduction of Mn(III)-TPP-*p*-CF_3 to Mn(II)-TPP-*p*-CF_3 was achieved after the addition of 10 equivalents (Figure 6a, THF) and 6 equivalents (Figure 6b, in DMSO), respectively. Re-oxidation was performed by leaving the samples in contact with atmospheric O_2 for both systems. As shown in Figure 7a and 7b, complete oxidation was observed for both systems after 1h, indicating the complete reversibility of the Mn(III)/(II)-TPP-*p*-CF_3 redox process.

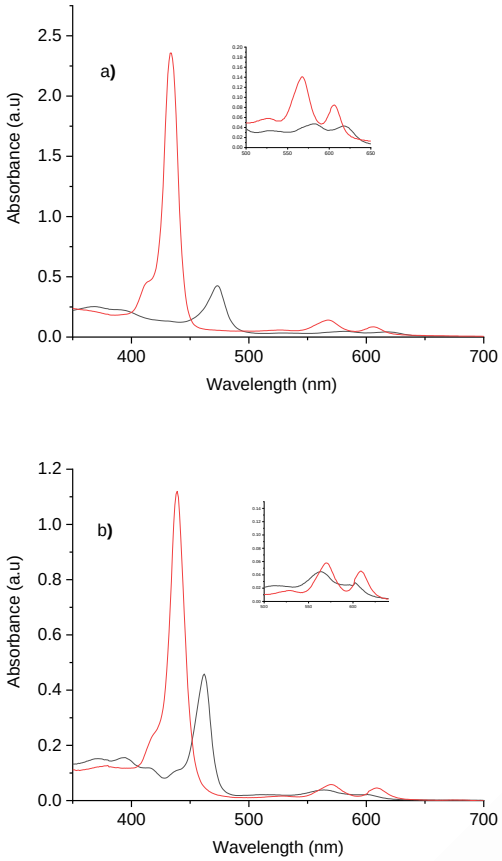

Figure 7. UV-Vis spectra showing the re-oxidation of Mn(II)-TPP-*p*-CF_3 upon air exposure after 1h, at 25°C: **a)** THF and **b)** DMSO, Mn(II)-TPP-*p*-CF_3 (red line), Mn(III)-TPP-*p*-CF_3 obtained after air exposure (black line).

In order to determine the empirical rate law for the reduction of Mn(III)-TPP-*p*-CF_3 by ascorbic acid, a series of kinetic experiments was conducted, at 25°C, in the absence of oxygen and under pseudo-first order conditions, following the disappearance of the Soret band at 473 nm (ε=1.65×10^5 M^{-1} s^{-1}) over time, at 500 ms intervals. Mn(III)-TPP-*p*-CF_3 concentrations were determined using the molar absorption coefficient (ε=1.65×10^5 M^{-1} s^{-1}) and the relationship between absorbance and concentration ($A = \varepsilon bc$-Beer-Lambert law). We assumed, like in previous studies [18], that the reduction obeyed second order kinetics (Figure S7a to d). Initial reaction rates were measured at two different ascorbic acid concentrations (0.6 mM and 1.25 mM) keeping the initial Mn(III)-TPP-*p*-CF_3 constant at 0.05 mM (Figure S5).The experimental data evidenced that the reduction reaction rate is first order in relation to Mn(III)-TPP-*p*-CF_3 displaying an overall second order constant of k_2≈127 ± 5 $M^{-1}s^{-1}$ and half-life ($t_{1/2}$) of 8.3 s and 0.6 s at total ascorbic acid concentrations of 0.6 mM and 1.25 mM, respectively. The k_2 value of Mn(III)-TPP-*p*-CF_3 (in the absence of oxygen) is about three times higher than the second order constant of k_2≈ 46 ± 5 $M^{-1}s^{-1}$ obtained earlier by us for the Mn(III) pegylated perfluorinated porphyrin Mn(III)-TPFPP(PEG)$_4$,[18] indicating faster reduction by ascorbate Under normal blood plasma concentrations of ascorbic acid, which are in the 20-40 µM range,[68,69] the calculated $t_{1/2}$ value for Mn(III)-TPP-*p*-CF_3 is in the 14-27 s range, compared with the range of $t_{1/2}$ values of 6-13 min for Mn(III)-TPFPP(PEG)$_4$ in the same conditions.[18] Moreover, ascorbic acid accumulates in circulating immune cells, reaching up to 1.2-3.5 mM concentrations[69] giving an intracellular half-life for Mn(III)-TPP-*p*-CF_3 of 0.4-4.6 s, shorter than the range reported for Mn(III)-TPFPP(PEG)$_4$,[18] if these complexes could enter those cells.

We note that no reduction of Mn(III)-TPP-*p*-CF_3 is observable with glutathione, even in a large excess of this reducing agent, similarly to what was reported for Mn(III)-TPFPP(PEG)$_4$.[18] This is likely the consequence of the coordination of the glutathione carboxylate groups to Mn^{III} in the axial position, as previously evidenced for Mn(III)-TPFPP(PEG)$_4$ by NMR data. It was suggested that the formation of the glutathione-porphyrin Mn(III) ternary complex prevents the electron transfer between the thiol group and the metal center.

Reduction of Mn(III)-TPP-p-CF_3 followed by ^{19}F NMR

The reduction of Mn(III)-TPP-*p*-CF_3 to Mn(II)-TPP-*p*-CF_3 using ascorbic acid in PBS (pH= 7.4) was also followed by ^{19}F NMR. As expected, upon reduction, the stronger paramagnetic relaxation effect of Mn(II) caused the disappearance of the broad ^{1}H signal of Mn(III)-TPP-*p*-CF_3 at δ=7.85 ppm. In the ^{19}F NMR spectrum (Figure 8), addition of 0.5 equivalents of ascorbate led to the appearance of a second, broader signal at -59.6 ppm, belonging to Mn(II)-TPP-*p*-CF_3, ~2 ppm apart from the ^{19}F signal of Mn(III)-TPP-*p*-CF_3 (δ= -61.11 ppm). The broadening of the signal for Mn(II)-TPP-*p*-CF_3 is in accordance with the more important T_2 shortening of Mn(II). Addition of 1.0 equivalent of ascorbate results in complete reduction of Mn(III)-TPP-*p*-CF_3 at this concentration (1.6 mM), evidenced by the complete disappearance of the Mn(III)-TPP-*p*-CF_3 ^{19}F peak in the spectrum. Reoxidation of Mn(II)-TPP-*p*-CF_3 to Mn(III)-TPP-*p*-CF_3 occurs with air oxygen and can be followed in time by ^{19}F NMR (Figure 8).

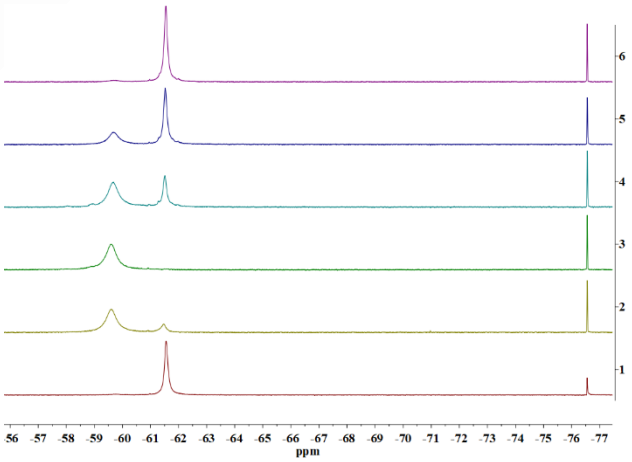

Figure 8. Reduction of Mn(III)-TPP-*p*-CF_3 with ascorbate and reoxidation of Mn(II)-TPP-p-CF_3 with air, as followed by ^{19}F NMR; c_{MnL}= 1.6 mM. 1) Mn(III)-TPP-*p*-CF_3 dissolved in 0.6 ml DMSO and 10 µl H_2O; 2) Mn(III)-TPP-*p*-CF_3 + 0.5 equ. ascorbate; 3) Mn(III)-TPP-*p*-CF_3 + 1.0 equ. ascorbate; 4) Mn(II)-TPP-*p*-CF_3 exposed to air for 1 h; 5) Mn(II)-TPP-*p*-CF_3 exposed to air for 4 h; 6) Mn(II)-TPP-*p*-CF_3 exposed to air for 1 day. The peak at -76.55 ppm corresponds to NaTFA as reference.

In order to further visualize the redox-dependent changes, phantom ^{19}F MR images have been acquired for the oxidized and reduced forms at 7 T, in DMSO. As a consequence of the shorter

T_2, MRI signal intensity becomes considerably weaker for the reduced sample, with a three-fold decrease in the signal to noise ratio (SNR). Reoxidation of the sample in open air can be also monitored on the ^{19}F MRI phantom images. Under our experimental conditions, complete oxidation occurred in ~24 hours. The ^{19}F signal intensity of the sample is progressively increasing upon oxidation, with a SNR which is linearly proportional to the percentage of Mn(III)-TPP-*p*-CF_3, as it is determined from integration of ^{19}F NMR spectra recorded in parallel on the same samples (Figure 9b).

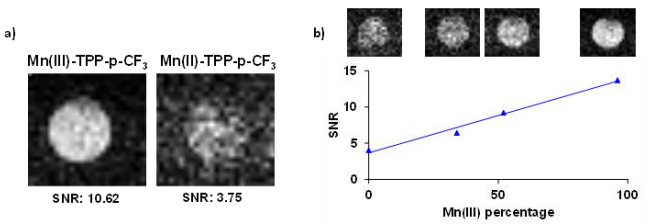

Figure 9. a) ^{19}F MRI phantom images acquired at 1.1 mM Mn(III)/(II)-TPP-*p*-CF_3 concentration in DMSO. b) Monitoring reoxidation of Mn(II)-TPP-*p*-CF_3 (c_{MnL}= 1.6 mM) by air oxygen: signal to noise ratio (with respect to the Mn(III)-TPP-*p*-CF_3 peak) as a function of the oxidized Mn(III)-TPP-*p*-CF_3 content (%); the signal of the Mn(II) complex was saturated with a selective pulse.
B = 7T; TR: 60 ms; TE: 1.3 ms; FA: 90°; NA: 256; acquisition time 8 min 11 s.

^{1}H relaxivity

Both +2 and +3 redox forms of manganese are paramagnetic in the high spin state and can be efficient relaxation agents. In particular, Mn(II) complexes are extensively explored as potential contrast enhancing probes for ^1H MRI, but Mn(III) chelates also attract considerable attention.[70,71,72] Although the Mn(III)/(II)-TPP-*p*-CF_3 chelates are not soluble in pure water, it seemed interesting to compare the relaxation properties of the two oxidation states in mixed DMSO/water (20/80) solvent. In the presence of water, two water molecules are expected to coordinate to the metal in axial positions in both Mn(III)/(II)-TPP-*p*-CF_3, as in typical porphyrin complexes of Mn(II) and Mn(III). The NMRD profiles recorded at 25°C for Mn(III)/(II)-TPP-*p*-CF_3 are shown in Figure 10. The reduction results in a change in the electronic structure of Mn from the $3d^4$ to the much more symmetrical $3d^5$ configuration, and this is accompanied by a change in the form of the NMRD curves. The profiles of Mn(II) and Mn(III) porphyrins usually cross each other and the relaxivity difference between the two oxidation forms can be largely field-dependent. Typically, small molecular weight porphyrin Mn(II) complexes display higher relaxivities at low fields, while their Mn(III) analogues have a characteristic high-field relaxivity peak between 10-100 MHz. The NMRD profiles of Mn(III)-TPP-*p*-CF_3 and Mn(II)-TPP-*p*-CF_3 show the same tendency; however, the absolute values of the relaxivities for both forms are very low, for instance above 10 MHz, they are approximately 4 times lower than those previously measured for PEGylated porphyrin Mn(II) and Mn(III) complexes.[18] The relaxivity is also highly dependent on the concentration: for Mn(III)-TPP-*p*-CF_3, dilution from 3.24 to 1.95 mM results in a ~50% relaxivity increase at all fields. Similarly low relaxivities have been previously reported for some Mn(III) porphyrin complexes, like the protoporphyrin Mn(III)-PP (8,13-divinyl-3,7,12,17-tetramethyl-21//,23Ff-porphine-2,l 8-dipropionic acid]manganese(III) chloride) or Mn(III)-CPI (3,8,13,18-tetramethyl-2l//,23/f-porphine-2,7,12,17-tetrapropionic acid]manganese(III) chloride), and their low values have been related to substantial aggregation.[73] Aggregation is a well-known phenomenon for porphyrins, where van der Waals forces operate to hold two or more molecules together. For Mn(III)-PP and Mn(III)-CPI, Kellar et al. associated this large relaxivity decrease in the aggregated form with respect to monomer Mn(III) porphyrins to a close Mn(III)-Mn(III) proximity making metal-metal interactions possible.[73] While the electronic relaxation times might not be significantly altered in homodinuclear species even if strong magnetic coupling occurs, such effects can alter the interaction between the paramagnetic ions and the protons they relax.[74,75] Moreover, in a face-to-face aggregated structure, where one porphyrin is stacked directly above the other, the coordination of the water molecule or its sufficiently fast exchange can be also prevented. Since proton relaxivity is linearly proportional to hydration number, this effect would diminish relaxivity in the same proportion in the entire frequency range. As shown in Figure 9, dilution of the Mn(III)-TPP-*p*-CF_3 sample breaks up aggregates and leads to a partial recovery of the relaxivity values, in a similar way as it was reported by Kellar et al. upon adding acetone to aggregated Mn(III) porphyrin solutions. It seems difficult to analyse more in details the ^1H relaxation effects. Nevertheless, we can conclude that porphyrin aggregation strongly limits proton relaxivities under our experimental conditions, and that, at most frequencies, there is an important difference between the two oxidation states in terms of the shape of the NMRD profiles and of the absolute relaxivity values.

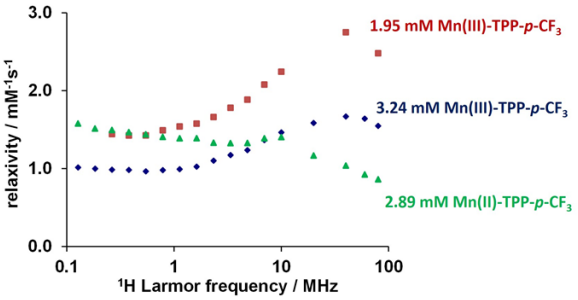

Figure 10. ^1H NMRD profiles recorded at 298 K in 20% DMSO and 80% water mixture for Mn(III)-TPP-*p*-CF_3 at 3.24 mM (blue ♦) and 1.95 mM (red ■) concentrations and for Mn(II)-TPP-*p*-CF_3 at 2.98 mM concentration (green ▲).

Antiproliferative effect of Mn(III) -TPP-p-CF_3 porphyrin

Despite having a low solubility in water, which renders the complex unsuitable as a MRI contrast agent, the Mn(III)-TPP-p-CF_3 porphyrin was assessed regarding its antiproliferative effect on the Caco-2 cell line, through the SRB assay (results expressed as a percentage of the control at time 0 h, Figure 11) using a very low percentage of DMSO in order to attain a high enough solubility (up to 5 µM). Overall, the Mn(III)-TPP-*p*-CF_3 complex was not found to exert a significant impact on this cell line. However, a higher effect was seen for the lowest and highest concentrations at all time points. This is still unexplained, and requires further biological tests in order to determine whether it may be due to a cellular accommodation to the intermediate concentrations of the Mn-complex. Moreover, longer exposure periods should be probed, with a view to assess the complex´s impact on cellular function.

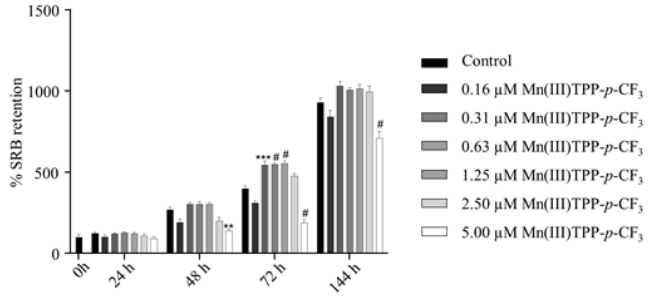

Figure 11. Effect of Mn(III)-TPP-*p*-CF_3 on the Caco-2 cell line, assessed by the SRB colorimetric assay. 72 hours after the addition of Mn(III)-TPP-*p*-CF_3, the medium was discarded and new culture medium was added. Results are represented as mean ± SD of three independent experiments (n = 3), performed in triplicate for each experimental condition. Data were analyzed using the one-way ANOVA method followed by the Tukey's multiple comparison test: p* < 0.05; p** < 0.01; p*** < 0.001; p# < 0.0001 were considered statistically significant. If p > 0.05, no statistically significant differences were considered.

Regarding the reversibility study, cellular proliferation increased significantly over time even after removal of the compound from the culture medium (up to 72 h). Therefore, in the presence of Mn(III)-TPP-*p*-CF_3 the cells appear to sense a significant effect at longer times (> 3 days), even when not in contact with the compound. This interesting behavior may indicate a long-term impact, but further studies are needed in order to validate this hypothesis. In any case, the existence of many FDA-approved CF_3 containing drugs[76] indicate that these substituents present in Mn(III)-TPP-*p*-CF_3 do not induce toxicity.

Conclusion

In the quest for responsive MRI agents that can provide a dual ^1H and ^{19}F MRI response to biological redox stimuli, we have synthesized a novel fluorinated manganese porphyrin, (Mn-TPP-*p*-CF_3). Although the complex has low water solubility, its full characterization by combined experimental and theoretical methods gives interesting insights into the structural design requirements of such imaging probes. ^{19}F relaxation time measurements for the non-metalated porphyrin as well as for the Mn(III) and Mn(II) oxidation states of Mn-TPP-*p*-CF_3 show the different paramagnetic effect of the two metal ions to accelerate relaxation. Mn(III)-TPP-*p*-CF_3 provides a favorable ratio of transverse and longitudinal ^{19}F relaxation times, with $T_2/T_1 = 0.61$, avoiding excessive line-broadening that would prevent efficient ^{19}F signal detection. This is related to the appropriate Mn(III)-F distances (d_{Mn-F} = 9.7-10 Å) as estimated by DFT calculations. Mn-TPP-*p*-CF_3 has a reversible Mn(II)/Mn(III) redox potential of -0.574 V vs. NHE. Fully reversible redox transformation of Mn-TPP-*p*-CF_3 between Mn(III)/Mn(II) oxidation states can be generated by ascorbate (reduction) and air oxygen (oxidation). These processes can be monitored via the charge transfer Soret bands of the Mn(III) and Mn(II) porphyrins in UV-Vis spectroscopy, the ^{19}F NMR signals observable for both oxidized and reduced forms, or the signal intensity changes in ^{19}F MRI phantom images. Proton relaxivities recorded for the Mn(III)/(II)-TPP-*p*-CF_3 chelates in mixed DMSO/water (20/80) solvent reflect the typical shape of Mn(II) and Mn(III) porphyrins, however, with very low absolute values related to aggregation.

Based on these results, and in particular the appropriate Mn(III)-F distance and related relaxation properties, Mn-TPP-*p*-CF_3 is an interesting core structure for the development of redox MRI probes, though further modifications are required to make it fully water-soluble. Previous experience shows that the integration of charged groups or PEG chains on the porphyrin are viable solutions to achieve this.

Experimental Section

Materials and Methods

Commercially available reagents were purchased from Aldrich, and used as received. All solvents were pre-dried according to standard laboratory techniques. For the cell culture and *in vitro* assays, antibiotics (penicillin–streptomycin 100x solution, ethylenediaminetetraacetic acid (EDTA, disodium salt, dihydrate), Minimum Essential Medium (MEM), MEM non-essential aminoacids solution (NEAA, 100x), phosphate buffered saline (PBS), sodium pyruvate solution (100 mM), trypan blue (0.4%), trypsin (10x solution, 25 g porcine trypsin *per* liter in 0.9% sodium chloride), and inorganic salts and acids (of analytical grade) were purchased from Sigma-Aldrich Chemical S.A. (Sintra, Portugal). Fetal bovine serum (FBS) was obtained from Gibco-Life Technologies (Porto, Portugal). The epithelium-like Caco-2 (Cancer coli-2) cell line, from human colorectal adenocarcinoma[76], was obtained from the European Collection of Cell Cultures (ECACC 09042001, Salisbury, UK).

UV-Vis absorption spectra were recorded on a Hitachi U-2010 using quartz cells. ^1H NMR and ^{19}F NMR spectra were recorded on a Bruker Avance III 400 MHz NMR spectrometer (^1H and ^{19}F frequencies of 400.101 and 376.5 MHz, respectively). Mass spectra (ESI-FIA-TOF) were acquired using Applied Biosystems Voyager DE-STR instrument equipped with a nitrogen laser (λ=337 nm).

Synthesis

5,10,15,20-tetrakis(4-trifluoromethylphenyl)porphyrin, TPP-p-CF_3 (1)

The synthesis of 5,10,15,20-tetrakis(4-trifluoromethylphenyl)porphyrin (1) was carried out according to the NaY/nitrobenzene methodology[55,56].A mixture of acetic acid (210 mL) and nitrobenzene (70 mL) was introduced in a round bottom flask. Then, NaY (20 g) and 4-(trifluoromethyl)benzaldehyde (8.18 mL, 0.06 mol) were added and the reaction was stirred at 120ºC for 20 minutes. 1*H*-Pyrrole (4.1 mL, 0.06 mol) was added dropwise and the reaction was stirred for two hours under reflux. Then, the hot suspension was filtered and the resulting solid material was washed with THF. To induce precipitation from the recovered liquid, methanol was added and then the solid was filtered using vacuum filtration. The resulting pure porphyrin was obtained in 20% yield. ^1H NMR (400 MHz, DMSO-d_6) δ ppm: 8.82 (s, $8H_\beta$), 8.34 (d, *J*=8Hz $8H_{Ar}$), 8.05 (d, *J*=8Hz $8H_{Ar}$), -2.80 (s, $2H_{NH}$); ^{19}F NMR (376.5 MHz, DMSO) δ ppm: -61.04 (s, 12 F); HRMS (ESI-TOF) m/z: calculated for $C_{48}H_{26}F_{12}N_4$: 886.2036, obtained 887.4532 $[M+H]^+$. IV falta introduzir

UV-Vis (THF): λ_{abs}, nm (ε, M^{-1} cm^{-1}): 418 ($3.3x10^5$); 512 ($1.7x10^4$); 546 ($5.8x10^3$); 589 ($5.1x10^3$); 645 ($2.5x10^3$).

Mn(III)-5,10,15,20-tetrakis(4-trifluoromethylphenyl)porphyrin, Mn(III)-TPP-p-CF_3 (2)

Porphyrin TPP-*p*-CF_3 **1** (100 mg, 0.113 mmol), manganese acetate (II) (156 mg, 0.903 mmol) and sodium acetate (370 mg, 0.451 mmol) were dissolved in acetic acid (3 mL). The mixture was stirred for two hours at 80ºC and controlled by UV-Vis spectroscopy. After complete conversion into the porphyrin complex Mn(III)-TPP-*p*-CF_3 **2**, the reaction mixture was dissolved in 5mL CH_2Cl_2 and the crude washed several times with H_2O (5mL) to remove the excess of salt. The organic layer was dried over anhydrous sodium sulfate and concentrated under vacuum. The resulting pure porphyrin was obtained in 85% yield. HPLC showed that the purity of the obtained porphyrin was 98%. ^{19}F NMR (376.5 MHz, DMSO) δ ppm: -61.56 (s, 12 F). HRMS (ESI-TOF) m/z: calculated for $C_{48}H_{26}F_{12}MnN_4$: 941.13, obtained 941.1254. UV-Vis (THF): λ_{abs}, nm (ε, M^{-1} cm^{-1}): 473 ($1.65x10^5$); 584 ($7.8x10^3$); 619 ($7.7x10^3$)
Falta introduzir IVFigure S1 shows the MS spectrum of the porphyrin Mn(III)-TPP-*p*-CF_3. Figure S2 shows HPLC chromatogram and Figure S3 shows the IV.

^{1}H and ^{19}F NMR study

^1H NMR spectra were measured in $CDCl_3$ for TFPP but Mn(III)-TFPP and TPP-*p*-CF_3 **1** in DMSO-d_6. ^{19}F NMR spectra were acquired only in $CDCl_3$ for Mn(III)-TFPP, in CDCl3 and DMSO for TFPP**,** but only in DMSO for TPP-*p*-CF_3 **1** and Mn(III)-TPP-*p*-CF_3 **2**. In the reduction and reoxidation experiment, the solution of Mn(III)-TPP-*p*-CF_3 **2** (1.6 mM) was prepared in DMSO. The reduction of Mn(III) to Mn(II) was achieved by adding ascorbate in PBS (pH = 7.4) and was followed by ^{19}F NMR spectroscopy (9.4 T Bruker Avance III NMR spectrometer) at room temperature (25 ˚C). Proton and ^{19}F chemical shifts are given in parts per million (ppm) relative to tetramethylsilane (TMS) and sodium trifluoroacetate (NaTFA) in D_2O, respectively. TMS was used as internal standard (δ 0.00 ppm for ^1H) and NaTFA was used in an insert tube (-76.55 ppm for ^{19}F).

^{19}F NMR Relaxometry

Solutions of TFPP, TPP-*p*-CF_3 **1**, Mn(III)-TPP-*p*-CF_3 **2** (c= 1.6 mM) and Mn(II)-TPP-*p*-CF_3 (1.1 mM; received by the reduction of Mn(III) complex) were prepared in $CDCl_3$ and DMSO. Their longitudinal and transverse ^{19}F relaxation times were measured on the 400 MHz Bruker Avance III NMR spectrometer ($\nu_{(19F)}$ = 376.5 MHz, 25 ºC). An inversion recovery pulse sequence was used for T_1 determination and a CPMG spin-echo sequence to determine T_2.

Cyclic Voltammetry

Owing to low aqueous solubility, the Mn(III)-TPP-*p*-CF_3 **2** stock solution was prepared by dissolving the solid compound in a mixture of 0.1 M HEPES buffer (pH 7.4) in water (as supporting electrolyte) and THF (500 µL THF + 1 mL buffer; HEPES = N-[2-hydroxyethyl]piperazine-N′-[2-ethanesulfonic acid] hemi-sodium salt; Sigma, St Louis, USA). Millipore Milli-Q nanopure water (resistivity ≥ 18 MΩ cm) was used for the preparation of the buffer solution. All experiments were performed at room temperature (25 ± 1 °C). pH measurements were carried out with a CRISON 2001 micro pH-meter (Crison, Spain).

Cyclic voltammetry (CV) measurements were carried out with an Ivium CompactStat potentiostat (Ivium Technologies, Netherlands) controlled by IviumSoft software (version 2.024). The electrochemical cell, volume 2 mL, contained a glassy carbon electrode (GCE), *d* = 1 mm (EDAQ, France) as the working electrode, a platinum wire as counter electrode and an Ag/AgCl (3 M KCl) reference electrode. Prior to the CV measurements, all solutions were degassed by N_2 bubbling for 15 min and during potential cycling a flux of N_2 was kept flowing on top of the cell solution.
All the potentials obtained were corrected to be reported in relation to the normal hydrogen electrode (NHE).

UV-Vis reduction study/Reduction kinetics

A stock solution of ascorbic acid (c=6.76 mM) in PBS and stock solutions of Mn(III)-TPP-*p*-CF_3 **2** in THF and DMSO (c=0.004 mM) were prepared. The reduction study was monitored by UV-Vis spectroscopy by adding different volumes of ascorbic acid to the stock solution of Mn(III)-TPP-*p*-CF_3 placed in the quartz cell. For the reduction kinetics experiment, the final concentration of Mn(III)-TPP-*p*-CF_3 **2** was kept at 0.05 mM . Two experiments were performed by adding 12 equivalents (corresponding to 0.6mM in the cuvette) of a stock solution of ascorbic acid in PBS and 25 equivalents of ascorbic acid (corresponding to 1.25mM in the cuvette). The conversion of Mn(III)-TPP-*p*-CF_3 **2** to Mn(II)-TPP-*p*-CF_3 was monitored by the disappearance of a strong UV-Vis absorbance band at 473 nm (ε=1.64×10^5 $M^{-1}s^{-1}$) which is absent in the UV-Vis spectrum of the Mn(II) complex. The decrease of the absorbance at 473 nm of the Mn(III) porphyrin in the presence of excess ascorbic acid, with the concomitant appearance of a new band characteristic of the Mn(II) porphyrin spectrum, was monitored over time. All the solutions used were argon de-aerated and measured in a sealed cuvette. The experimental setup used to monitor the kinetics of the reaction consisted of a fiber coupled Ocean Optics spectrometer (USB4000-UV-Vis) used in absorption mode together with a MiKropack DH-2000-BAL UV-Vis-NIR light source. The absorption spectra were recorded at intervals of 500 ms and monitored up to complete formation of the Mn(II) porphyrin species.

Theoretical calculations

Quantum chemical calculations were carried out in order to assess the F-Mn(III) distance in Mn(III) porphyrins, which is important for the ^{19}F relaxation rates. The structure and the preferred conformations of Mn(III)-TPP-*p*-CF_3 were investigated. For a comparison, another Mn(III) porphyrin complex, Mn(III)-TFPP, was also included in this study (name, structure and ^{19}F NMR characterization shown in Fig S4, S5). The structure of these complexes was optimized at the DFT level using the B3LYP[77,78,79] hybrid functional and the 6-31G(d,p) basis set. The most stable arrangements of the *ph*-CF_3 and *ph*-F groups around the C-C bond that defines their orientation relative to the porphyrin plane were explored considering different starting structures. Calculations were performed using the Gamess[80] program package. Graphical representations were produced with Gaussview.

^{1}H NMRD measurements

Relaxometric measurements of both Mn(II) and Mn(III) porphyrin complexes were carried out in 20% DMSO-80% H_2O mixtures at

1.95 and 3.24 mM for Mn(III)-TPP-*p*-CF_3 and 2.89 mM for Mn(II)-TPP-*p*-CF_3. The Mn(II)-TPP-*p*-CF_3 sample was obtained by reduction of a Mn(III)-TPP-*p*-CF_3 solution prepared in DMSO, by addition of 12 equivalents of ascorbic acid solution (0.19 M, prepared in aqueous PBS, pH 7.4). Complete reduction was verified by recording UV-Vis spectra. ^{1}H NMRD (Nuclear Magnetic Relaxation Dispersion) profiles of Mn(II)-TPP-*p*-CF_3 and Mn(III)-TPP-*p*-CF_3 solutions were recorded on a Stelar SMARtracer Fast Field Cycling NMR relaxometer (0.01-10 MHz) and a Bruker WP80 NMR electromagnet (20, 40, 60 and 80 MHz) adapted to variable field measurements and controlled by a SMARtracer PC-NMR console. The temperature was monitored by a VTC91 temperature control unit and maintained by a gas flow. The temperature was determined by previous calibration with a Pt resistance temperature probe. The longitudinal proton relaxation rates ($1/T_1$) were determined in water at 25 ^{o}C.

^{19}F MRI

^{19}F MRI measurements on tube phantoms of 250 µl volume were conducted on a Bruker 7 T PharmaScan Bruker spectrometer, using a home-made loop-gap coil and FLASH pulse sequence with the following parameters: flip angle 90°; TR 60 ms; TE 1.3 ms; field of view 1.28 cm × 1.28 cm; slice thickness 2 mm; number of averages 256; reconstruction/acquisition matrix 32 × 32; measurement time 8 min 11 s. Phantom ^{19}F MRI images on Mn(III)-TPP-*p*-CF_3 and Mn(II)-TPP-*p*-CF_3 were recorded at 1.1 mM concentration. The Mn(II)-TPP-*p*-CF_3 complex was obtained by reduction of a Mn(III)-TPP-*p*-CF_3 solution prepared in DMSO, by addition of 12 equivalents of ascorbic acid solution (0.19 M, prepared in aqueous PBS, pH 7.4). Re-oxidation of the Mn(II)-TPP-*p*-CF_3 complex was investigated at 1.6 mM concentration. During the re-oxidation measurements, the signal of the Mn(II) complex was saturated with a selective pulse (length: 4 ms duration, bandwith: 320 Hz; offset: 645 Hz; amplitude 5 µT; 1 pulse, magnetization transfer module). The signal to noise ratio was calculated using the following equation: $SNR = [2 \times ((signal)^2 - (noise)^2)/ (noise)^2]^{1/2}$.[81]

In vitro Assays

Cell Culture

The human Caco-2 epithelium cell line, from colorectal adenocarcinoma, was used in this study. The cells were cultured as monolayers at 37 °C, in a humidified atmosphere of 5% CO_2. The cultures were maintained in MEM medium supplemented with 10% *(v/v)* heat-inactivated FBS, 1% (v/v) NEAA, 1% (v/v) sodium pyruvate, 1% *(v/v)* penicillin (100 U/mL)/streptomycin (100 mg/mL) and sodium bicarbonate-20 mM (pH 7.4). Cells were sub-cultured at 80% confluence, using trypsin-EDTA (1x). Under these conditions, the duplication time was around 24 h. The cells were always in the logarithmic phase of growth when the tested agents were added.

Evaluation of Antiproliferative Effect

Cell density was evaluated by the SRB[82] assay, yielding the antiproliferative ability of the Mn(III)-TPP-*p*-CF_3 complex. Untreated cell cultures (control samples) were also assessed at the same time points. The tested compound was solubilized in water with a maximum of 10% DMSO, yielding a final concentration of 0.01% of DMSO. Controls were also tested at this final concentration. For the SRB assay, the cells were seeded in 24 wells at a density of $3x10^4$ cells/cm^2, treated with different concentrations of the tested compound and monitored over time – after 24, 48 and 72 h of exposure. In addition, a reversibility study was carried out, by removing the medium containing the tested agent after 72 h and substituting it by new culture medium, after which the cells were left to incubate for 72 h (a total of 144 h). Cell density was measured at each time point.

Supporting Information

Supporting Information is available. NMR, mass spectrum, additional cyclic voltammograms, kinetic experiments, electronic structure calculations.

Acknowledgements

This work was supported by FCT (Fundação para a Ciência e Tecnologia), QREN/FEDER (COMPETE Programa Operacional Factores de Competitividade) through projects UIDB/00070/2020, UIDP/00070/2020, UIDB/00313/2020, UIDP/00313/2020 and UIDB/00285/2020, and by the French Academy of Science *via* the Prix Mariano Gago 2022. The authors thank Dr Frédéric Szeremeta for recording the MRI phantom images and acknowledge the Mo2ving platform (Centre of Molecular Biophysics, Orléans) for access to the MRI facility and the Portuguese NMR Network for access to the UC-NMR facility which is supported in part by FEDER – European Regional Development Fund through the COMPETE Programme (Operational Programme for Competitiveness) and by National Funds through FCT – Fundação para a Ciência e a Tecnologia (Portuguese Foundation for Scie
nce and Technology) through grants RECI/QEQ-QFI/0168/2012, CENTRO-07-CT62-FEDER-002012, and also through support to Rede Nacional de Ressonância Magnética Nuclear (RNRMN) and to Coimbra Chemistry Centre through grant UID/QUI/00313/2019. Zoltán Garda has received funding from the European Union's Horizon 2021 research and innovation programme under the Marie Skłodowska-Curie grant agreement No. 101065389.

Keywords: Porphyrin; Fluorine; Redox Probe; ^{19}F MRI; NMR Relaxometry, manganese

[1] D.F. Quail, J.A. Joyce, *Nat. Med.* **2013**, 19, 1423-1437.
[2] N.W. Lutz, Y.Le Fur, J. Chiche, J.Pouyssegur, P.J. Cozzone, *Cancer Res*., **2013**, 73, 4616-4628.
[3] A. Rubartelli, M.T. Lotze, *Trends Immunol*., **2007**, 28, 429-436.
[4] D.J. Hausenloy, D.M. Yellon, *J. Clin. Invest*. **2013**, 123, 92-100.
[5] E.H. Sarsour, M.G. Kumar, L. Chaudhuri, A.L. Kalen, P.C. Goswami, *Antioxid. Redox Signaling* **2009**, 11, 2985-3011.
[6] V. Mirabello, F. Cortezon-Tamarit, S.I. Pascu, *Front. Chem.* **2018**,6, 27.
[7] T. Yoshihara, Y. Hirakawa, M. Hosaka, M. Nangaku, S. Tobita, *J. Photochem.* **2017**, 30, 71-95.
[8] I.N. Fleming, R. Manavaki, P.J. Blower, C. West, K.J. Williams, A.L. Harris, J. Domarkas, S. Lord, C. Baldry. F.J. Gilbert, *British Journal of Chemistry* **2015**, 112, 238-250.
[9] S.M.A. Pinto, V. Tomé, M.J.F. Calvete, M.M.C.A. Castro, E. Tóth, C. F.G.C. Geraldes, *Coord. Chem. Rev*., **2019**, 390, 1-31.

[10] M. Bourgeois, H. Rajerison, F. Guerard, M. Mougin-Degraef, J. Barbet, N. Michel, M. Cherel, A. Faivre-Chauvet, *Nucl. Med. Rev. Cent. East. Eur*., **2011**, 14, 90-95.
[11] K.A. Wood, W.L. Wong, M.I. Saunders, *Nucl. Med. Biol*., **2008**, 35, 393-400.
[12] J.A. Alawneh, R.R. Moustafa, S.T. Marrapu, U. Jensen-Kondering, R.S. Morris, P.S. Jones, F.I Aigbirhio, T.D. Fryer, T.A. Carpenter, E. A. Warburton, J.C. Baron, *Eur. J. Nucl. Med. Mol. Imaging*, **2014**, 41, 736-744.
[13] S.S. Xue, Y. Pan, W. Pan, S. Liu, N. Li, B. Tang, *Chem. Sci*., **2022**, 13, 9468-9484.
[14] C. Bonnet, E. Tóth, *Curr. Opin. Chem. Biol*., **2021**, 61, 154-169.
[15] J.R. Morrow, J.J. Raymond, M. Saiful, I. Chowdhury, P.R. Sahoo, *Inorg. Chem.*, **2022**, 61, 14487-14499.
[16] G.S. Loving, S. Murkherjee, P. Caravan, *J. Am. Chem. Soc*., **2013**, 135, 4620-4623.
[17] E.M. Gale, C.M. Jones, I. Ramsay, C.T. Farrar, P. Caravan, J. *Am. Chem. Soc*., **2016**, 138, 15861-15864.
[18] S.M.A. Pinto, M.J.F. Calvete, M.E. Ghica, S.Soler, I. Gallardo, A. Pallier, M.B.Laranjo, A.M.S. Cardoso, M.M.C.A. Castro, C.M.A. Brett, M.M. Pereira, E. Tóth, C.F.G.C. Geraldes, *Dalton Trans*., **2019**, 48, 3249-3262.
[19] J.C. Knight, P.G. Edwards, S.J. Paisey, *RSC Adv*., **2011**, 1, 1415-1425.
[20] I. Tirotta, V. Dichiarante, C. Pigliacelli, G. Cavallo, G. Terraneo, F.B. Bombelli, P. Metrangolo, G. Resnati, *Chem. Rev.*, **2015**, 115, 1106−1129.
[21] E. Hequet, C. Henoumont, R.N. Muller, S. Laurent, *Future Med. Chem*., **2019**, 11, 1157-1175.
[22] J. Ruiz-Cabello, B.P. Barnett, P.A. Bottomley, J.W. Bulte, *NMR Biomed*., **2011**, 24, 114-119.
[23] K.L. Peterson, K. Srivastava, V.C. Pierre, *Front. Chem*., **2018**, 6, 160.
[24] D. Xie, T.L. King, A. Banerjee, V. Kohli, E.L. Que, *J. Am. Chem. Soc*., **2016**, 138, 2937-2940
[25] K.H. Chalmers, E. De Luca, N.H.M. Hogg, A.M. Kenwright, I. Kuprov, D. Parker, M. Botta, J.I. Wilson, A.M. Blamire, *Chem. Eur. J*., **2010**, 16, 134-148.
[26] P. Harvey, I. Kuprov, D. Parker, *Eur. J. Inorg. Chem*. **2012**, 2012, 2015-2022.
[27] P. K. Senanayake, A. M. Kenwright, D. Parker, S. K. van der Hoorn, *Chem. Commun.* **2007**, 28, 2923-2925.
[28] K. Srivastava, G. Ferrauto, V. G. Young, Jr., S. Aime, V. C. Pierre, *Inorg. Chem*. **2017**, 56, 12206-12213.
[29] P. Kadjane, C. Platas-Iglesias, P. Boehm-Sturm, V. Truffault, G. E. Hagberg, M. Hoehn, N. K. Logothetis, G. Angelovski, *Chem. Eur. J.* **2014**, 20, 7351-7362.
[30] N. Cakic´, B. Tickner, M. Zaiss, D. Este-ban-Gómez, C. Platas-Iglesias, G. Angelovski, *Inorg. Chem*. **2017**, 56, 7737-7745.
[31] D. Xie, M.Yu, R.T. Kadakia, E.L. Que, *Acc. Chem. Res*. **2020**, 53, 2-10.
[32] D. Xie, S. Kim, V. Kohli, A. Banerjee, M. Yu, J.S. Enriquez, J.J. Luci, E.L. Que, *Inorg. Chem*., **2017**, 56, 6429-6437.
[33] R.T. Kadakia, D. Xie, H. Guo, B. Bouley, M. Yu, E.L. Que, *Dalton Trans*., **2020**, 49, 16419-16424.
[34] M. Yu, D. Xie, K.P. Phan, J.S. Enriquez, J.J. Luci, E.L. Que, *Chem. Commun.* **2016**, 52, 13885-13888.
[35] K. Tanaka, N. Kitamura, Y. Takahashi, Y. Chujo, *Bioorg. Med. Chem*. **2009**, 17, 3818–3823.
[36] L. A. Basal, M. D. Bailey, J. Romero, M. M. Ali, L. Kurenbekova, J. Yustein, R. G. Pautler, M. J. Allen, *Chem. Sci*., **2017**, 8, 8345-8350.
[37] H. Chen, X. Tang, X. Gong, D. Chen, A. Li, C. Sun, H. Lin, J. Gao, *Chem. Commun*., **2020**, 56, 4106-4109.
[38] M.J.F. Calvete, M. Piñeiro, L. D. Dias, M.M. Pereira, *ChemCatChem*, **2018**, 10, 3615-3635.
[39] G. Piccirillo, R.T. Aroso, F.M.S. Rodrigues, R.M.B. Carrilho, S.M.A. Pinto, M.J.F. Calvete, M.M. Pereira, *Catalysts*, **2021**, 11, 1335-1370.
[40] X. Li, H. Lei, L. Xie, N. Wang, W. Zhang, R. Cao, *Acc. Chem. Res.*, **2022**, 55, 878-892.
[41] C.A. Henriques, S.M.A. Pinto, J. Pina, C. Serpa, A. Fernandes, L.M. Rossi, M.F. Ribeiro, M.M. Pereira, M.J.F. Calvete, *Dalton Trans*. **2016**, 45, 16211-16220.
[42] A.T. Marques, S.M.A. Pinto, C.J.P. Monteiro, J.S.S. de Melo, H.D. Burrows, U. Scherf, M.J.F. Calvete, M.M. Pereira, *J.Polym.Sci Part A: Polym. Chem*., **2012**, 50, 1408-1417.
[43] J. Roales, J.M. Pedrosa, M.G. Guillen, T. Lopes-Costa, S.M.A. Pinto, M.J.F. Calvete, M.M. Pereira, *Sens. Actuators B.*, **2015**, 210, 28-35.
[44] R.T. Aroso, L.D. Dias, K.C. Blanco, J.M.Soares, F. Alves, G.J. da Silva, L.G. Arnaut, V.S. Bagnato, M.M. Pereira, *J. Photochem. Photobiol.B,* **2022**, 233, 11249.
[45] S.M.A. Pinto, S.F.F. Almeida, V.A. Tomé, A.D. Prata, M.J.F. Calvete, C. Serpa, M.M. Pereira, *Dyes Pigm.* **2021**, 195, 109677.
[46] L.B. Josefsen, R.W. Boyle, *Theranostics* **2012**, 9, 916-966.
[47] M.J.F. Calvete, S.M.A. Pinto, M.M. Pereira, C.F.G.C. Geraldes, *Coord. Chem. Rev.*, **2017**, 333, 82-107.
[48] S. Aime, M. Botta, E. Gianolo, E. Terreno, *Angew. Chem. Int. Ed.*, **2000**, 39, 747-750.
[49] D. Zhang, W. Lan, Z. Zhou, L. Yang, Q. Liu, Y. Bian, J. Jiang, *Top. Curr. Chem*. **2019**, 377, 1-43.
[50] L.J. Boucher, *Coord. Chem. Rev*. **1972**, 7, 289-329.
[51] K. Leung, C.J. Medforth, *Prepr. Arch. Condens. Matter*. **2007**, 1-10.
[52] C.F.G.C. Geraldes, M.M.C.A. Castro, J.A. Peters, *Coord.Chem.Rev*. **2021**, 445, 214069.
[53] E. M. Gale, S. Mukherjee, C. Liu, G. S. Loving, P. Caravan, *Inorg. Chem*. 2014, 53, 10748–10761
[54] I. Bertini, C. Luchinat, G. Parigi and E. Ravera, NMR of Paramagnetic Molecules - Applications to Metallobiomolecules and Models, Elsevier, Amsterdam, **2017**.
[55] M. Silva, A. Fernandes, S.S. Bebiano, M.J. Calvete, M.F. Ribeiro, H.D. Burrows, M.M. Pereira, *Chem. Comm*., **2014**, 50, 6571-6573.
[56] S.M.A. Pinto, C.A. Henriques, V.A. Tomé, C.S. Vinagreiro, M.J.F. Calvete, J.M. Dabrowski, M. Pineiro, L.G. Arnaut, M.M. Pereira, *J. Porphyr. Phthalocyanines* **2016**, 20, 1-16.
[57] T.R. Janson, L.J. Boucher, J.J. Katz, *Inorg. Chem*., **1973**, 12, 940-943.
[58] P. Turner, M.J. Gunter, *Inorg. Chem*., **1994**, 33, 1406-1415.
[59] W. Harhouri, S. Dhifaoui, Z. Denden, T. Roisnel, F. Blanchard, H. Nasri, *Polyhedron*, **2017**, 130, 127-135
[60] E. Sun, Y. Shi, P. Zhang, M. Zhou, Y. Zhang, X. Tang, T. Shi, *J. Mol. Struct*. **2008**, 889, 28-34.
[61] L. Ruhlmann, A. Nakamura, J. G. Vos, J-H. Fuhrhop. *Inorg. Chem*. **1998**, 37, 6052-6059.
[62] I. Bertini, L. Band, R.D. Brown, S.H. Koenig, *Inorg. Chem*., **1988**, 27, 951-953.
[63] G.R. Friedermann, M. Halma, K.A.D.F. Castro, F.L. Benedito, F.G. Doro, S.M. Drechsel, A.S. Mangrich, M.D. Assis, S. Nakagaki, *Appl. Catal. A: General*, **2006**, 308, 172-181.
[64] L.J. Boucher, *Coordin. Chem. Rev.*, **1972**, 7, 289-329
[65] I. Batinic-Haberle, A.Toymasyan, I. Spasojevic, Antioxid. Redox Signal, **2018**, 29, 1691-1724.
[66] A. Tovmasyan, T. Weitner, H. Sheng, M. Lu, Z. Rajic, D. S. Warner, I. Spasojevic, J. S. Reboucas, L. Benov, I. Batinic-Haberle, *Inorg. Chem*., **2013**, 52, 5677–5691.
[67] M. Velayutham, I. Batinic-Haberle, A. Tovmasyan, *Free Radic. Biol. Med*., **2016**, 100, S112.
[68] L. Robitaille, L.J. Hoffer, *Nutr. J.* **2016**, 15, 1-9.
[69] M. Levine, C. C. Cantilena, Y.H. Wang, R.W. Welch, P.W. Washko, K. R. Dhariwal, J.B. Park, A. Lazarev, J.F. Graumlich, J. King, L.R. Cantilena, *Proc. Natl. Acad. Sci. U.S.A*. **1996**, 93, 3704-3709.
[70] M. Botta, F. Carniato, D. Esteban-Gómez, C. Platas-Iglesias, L. Tei, *Future Med. Chem.* **2019**, 11, 1461-1483.
[71] A. Gupta, P. Caravan, W. S. Price, C. Platas-Iglesias, E. M. Gale, *Inorg. Chem.* **2020**, 59, 6648-6678.
[72] S. Lacerda, D. Ndiaye, É. Tóth, Manganese Complexes as Contrast Agents for Magnetic Resonance Imaging in “Metal Ions in Life Sciences” Eds: A. Sigel, E. Freisinger, R. K. O. Sigel © Walter de Gruyter GmbH, Berlin, Germany **2021**, 22, 71–99.
[73] K. Kellar, N. Foster, *Inorg. Chem.* **1991**, 31, 1353-13597
[74] I. Bertini, L. Band, R.D. Brown, S.H. Koenig, *Inorg. Chem*., **1988**, 27, 951-953.
[75] L. Band, L. Bertini, C. Luchinat, *Struct. Bonding*, **1990**, 72, 113-136.
[76] A. S. Nair, A. K. Singh, A. Kumar, S. Kumar, S. Sukumaran, V. P. Koyiparambath, L. K. Pappachen, T. M. Rangarajan, H. Kim, B. Mathew, *Processes*, **2022**, 10, 2054.
[77] J. Fogh, W.C. Wright, J.D. Loveless, *J. Natl. Cancer Inst*. **1977**, 58, 209-214.
[77] A.D. Becke, *Phys. Rev. A.* **1988**, 38, 3098−3100.
[78] A.D. Becke, *J. Chem. Phys*. **1993**, 98, 5648−5652.
[79] C. T. Lee, W. T. Yang, R. G. Parr, *Phys. Rev. B* **1988**, 37, 785−789.
[80] M. W. Schmidt, K. K. Baldridge, J. A. Boatz, S. T. Elbert, M. S. Gordon, J. H. Jensen, S. Koseki, N. Matsunaga, K. A. Nguyen, S. J. Su, T. L. Windus, M. Dupuis, J. A. Montgomery, *J. Comput. Chem*. **1993**, 14, 1347−1363.
[81] J. Blahut, K. Bernásek, A. Galisova, V. Heynek, I. Cisarova, J. Kotek, J. Lang, S. Matejkova, P. Hermnn, *Inorg. Chem*. **2017**, 56, 13377-13348.
[82] P. Skehan,R. Storeng, D. Scudiero, A. Monks, J. Mcmahon, D. Vistica, J.T. Warren, H. Bokesch, S. Kenney, M.R. Boyd, *J. Natl. Cancer Inst*. **1990**, 82, 1107–1112.